




Performance of Ni/10Sc1CeSZ anode synthesized by glycine nitrate process assisted by microwave heating in a solid oxide fuel cell fueled with hydrogen or methane

Abdul Azim Jais¹ · S. A. Muhammed Ali¹ · Mustafa Anwar² · Mahendra Rao Somalu¹  · Andanastuti Muchtar^{1,3} · Wan Nor Roslam Wan Isahak⁴ · Nurul Akidah Baharudin¹ · Kean Long Lim¹ · Nigel P. Brandon⁵

Received: 9 October 2019 / Revised: 9 January 2020 / Accepted: 2 February 2020 / Published online: 8 February 2020
© Springer-Verlag GmbH Germany, part of Springer Nature 2020

Abstract

Nickel/scandia-ceria-stabilized-zirconia (Ni/10Sc1CeSZ) cermet is a potential anode for solid oxide fuel cells. The anode powder is prepared through a microwave-assisted glycine nitrate combustion process, and its properties, including phase and chemical composition as well as morphology, are characterized by XRD, TEM, and EDS techniques. The electrical conductivity and electrochemical behavior under low concentration of dry hydrogen (H₂:N₂ volume ratio = 10:90) and dry methane (CH₄:N₂ volume ratio = 50:50) fuels are determined. XRD results show two phases, namely, cubic NiO phase and cubic 10Sc1CeSZ phase, with the crystallite sizes of 67 and 40 nm, respectively. The area specific resistances (ASRs) of the prepared anode measured using a symmetrical cell of Ni/10Sc1CeSZ|10Sc1CeSZ|Ni/10Sc1CeSZ are 0.96 and 24.3 Ω cm² observed at 800 °C in dry low hydrogen concentration (10 vol% hydrogen–90 vol% nitrogen) and dry methane (50 vol% methane–50 vol% nitrogen) fuels, respectively. The ASR in methane fuel is higher than that in hydrogen fuel at all operating temperatures (600–800 °C) because of carbon deposition. The amount of deposited carbon and degree of graphitization (I_G/I_D) of this anode after exposure in methane at 800 °C for 3 h are 4.34% and 2.1, respectively. Overall, Ni/10Sc1CeSZ cermet synthesized by glycine nitrate process assisted with microwave-heating technique exhibits acceptable electrochemical behavior even at low hydrogen concentration and also in dry methane. This can be related to the improved powder morphology as a result of uniform heating assisted by microwave energy.

Keywords Solid oxide fuel cell · Nickel/scandia-stabilized zirconia · Microwave heating, electrical conductivity · Electrochemical performance · Graphitization degree

✉ Mahendra Rao Somalu
mahen@ukm.edu.my

¹ Fuel Cell Institute, Universiti Kebangsaan Malaysia, 43600 UKM Bangi, Selangor, Malaysia

² US-Pakistan Center for Advanced Studies in Energy (USPCAS-E), National University of Sciences and Technology, NUST H-12, Islamabad 44000, Pakistan

³ Department of Mechanical and Manufacturing Engineering, Faculty of Engineering and Built Environment, Universiti Kebangsaan Malaysia, 43600 UKM Bangi, Selangor, Malaysia

⁴ Department of Chemical and Process Engineering, Faculty of Engineering and Built Environment, Universiti Kebangsaan Malaysia, 43600 UKM Bangi, Selangor, Malaysia

⁵ Department of Earth Science and Engineering, Imperial College London, South Kensington Campus, London SW7 2AZ, UK

Introduction

Solid oxide fuel cells (SOFCs) are promising electrochemical devices that produce electricity directly from the chemical energy of fuels (e.g., hydrogen and hydrocarbons) with a high efficiency of over 60% [1]. Nickel-based cermet is a commonly used SOFC anode material because of its high electronic conductivity, thermal compatibility with electrolyte component, excellent catalytic activity toward hydrogen-fuel oxidation, ability to directly catalyze hydrocarbon-fuel reforming, and low cost [2]. Nickel cermets such as nickel/yttria-stabilized zirconia (Ni/YSZ), nickel/scandia-stabilized zirconia (Ni/ScSZ), nickel/samarium-doped ceria (Ni/SDC), and nickel/gadolinium-doped ceria (Ni/GDC) have been progressively studied for SOFCs using various fuels including hydrogen, hydrocarbons, and ammonia, as well as for application in

intermediate-to-low-temperature SOFCs [3–9]. The catalytic activity of nickel toward hydrocarbon fuels such as methane enhances the formation of carbon, which is deposited onto the nickel surface and consequently blocks the gas-diffusion pores and effective hydrogen oxidation in the anode. As a result, SOFC performance is decreased by the deactivation of nickel cermet active sites for electrochemical catalytic activity. Nickel/scandia-ceria-stabilized zirconia (Ni/10Sc1CeSZ) is a promising anode material because carbon deposition is significantly less with this material than with Ni/YSZ and Ni/ScSZ equivalents [10].

Studies on the synthesis, development, and fabrication of anode components are gaining increased attention for the investigation of the optimum conditions under which anode and SOFC performance can be enhanced [3]. The electrode polarization of cermet anodes measured by electrochemical impedance spectroscopy (EIS) can be reduced by optimizing the microstructure, nickel–nickel contact, and porosity of anode. These features are inter-related with the initial powder properties, such as phase purity and particle size, which can be improved by synthesis or preparation methods. Various synthesis techniques such as solid-state reaction (SSR) [11, 12], solid–liquid method [13], co-precipitation [5], sol–gel method [14], impregnation method [15, 16], hydrothermal method [17], citrate-nitrate process [18], and glycine-nitrate process [4, 19–21] have been proposed to produce nickel cermet powders with improved properties. Recently, microwave-assisted techniques in the solution combustion synthesis and sintering processes have been developed and established as a potential technique to synthesize, prepare, and fabricate SOFC materials including anodes, cathodes, and ceramic electrolytes [22–28]. Microwave-assisted combustion is a rapid, effective method of preparing nanomaterials involving the auto-combustion of homogeneous metal nitrate solutions mixed with fuel (glycine, citrate, and urea). Microwave energy initiates a reaction that leads to solution combustion by providing uniform heating and accelerating the reaction rate [8, 29]. The rapid reaction for the combustion/ignition enhanced by microwave heating can produce powders with high crystallinity and purity in addition to uniform microstructure. The microwave-assisted technique is fast, practical, easy, simple, and energy saving. Thus, this technique has potential applications in the material-science field, specifically in producing nanostructured materials including metal oxides and other functional materials [30]. To date, significant studies on the microwave-assisted glycine-nitrate process for preparing cermet anode materials such as copper cermet anode (Cu/GDC) [31] and Ni/SDC [32] have been reported. However, the microwave-assisted solution combustion synthesis of Ni/10Sc1CeSZ cermet and its electrochemical behavior toward hydrogen and dry

methane fuels has not yet been reported to the best of our knowledge.

The present paper is aimed at exploiting the advantages of microwave-heating technique. Ni/10Sc1CeSZ cermet was synthesized through a microwave-assisted glycine nitrate process (MW-GNP), and its electrochemical behavior was evaluated in dry low hydrogen concentration and dry methane fuels at SOFC operating temperature. The phase formation, microstructure, porosity, and carbon deposition behavior of the prepared anode were also investigated. The area specific resistance (ASR) of the cermet was analyzed by EIS between 600 and 800 °C in dry low hydrogen concentration ($H_2:N_2$ volume ratio = 10:90) and dry methane ($CH_4:N_2$ volume ratio = 50:50) fuels using a symmetrical cell of NiO/10Sc1CeSZ|10Sc1CeSZ|NiO/10Sc1CeSZ. A cermet anode with 50 vol% Ni metal and 50 vol% 10Sc1CeSZ ceramic electrolyte was selected based on the percolation theory of nickel phase, which contributed sufficient electronic-conduction characteristic to the anode material.

Experimental procedures

Synthesis and characterization of NiO/10Sc1CeSZ powder

NiO/10Sc1CeSZ (NiO/10 mol% Sc_2O_3 –1 mol% CeO_2 –89 mol% ZrO_2) powder consisting of 50 vol% Ni and 50 vol% 10Sc1CeSZ was prepared via a glycine–nitrate combustion process (GNP) assisted with microwave heating technique. First, a clear scandium nitrate solution was obtained by dissolving proper amounts of scandium oxide (99.9% purity; Sigma-Aldrich, Germany) in a hot nitric acid solution (65% purity, reagent grade; Friendemann Schmidt, Australia). Second, stoichiometric amounts of nickel (II) nitrate hexahydrate (99% purity; Friendemann Schmidt, Australia), zirconium (IV) oxynitrate hydrate (99.5% purity; Acros Organics, Belgium), and cerium (III) nitrate hexahydrate (99%; Sigma-Aldrich, Germany) were separately dissolved in deionized water. The nitrate solution was then mixed with the solution of scandium nitrate to prepare a metal nitrate precursor solution. Next, a solid form of glycine (Biotech grade; GeneMark, Taiwan) as a fuel for the solution combustion reaction was added to the precursor solution. The molar fraction of glycine-to-nitrate ratio was 1:2 (in mole). The temperature of the mixed solution was constantly kept at 100 °C and stirred on a hot plate until a viscous solution was formed. The rapid and self-propagating-type combustion of the viscous solution was undertaken in a microwave oven (SHARP, 2.5 GHz) with output power setting of 720 W, which completely converted the sample into ash within 3 min. The resulting combustion ash was then fired in using a furnace (CWF1200, Carbolite, UK) at 800 °C of calcination temperature in air for 2 h. Finally,

NiO/10Sc1CeSZ anode powder was produced and powder characterization was conducted.

The phase of the synthesized NiO/10Sc1CeSZ powder was characterized by X-ray diffraction (XRD) by using an X-ray diffractometer (D8 Advance, Bruker; wavelength of Cu-K α X-ray = 0.1542 nm; $2\theta = 20^\circ$ – 90°). The XRD of powder was performed at room temperature. X'Pert HighScore Plus software was used to analyze the XRD data, and the Rietveld refinement was conducted to obtain the lattice parameter and crystallite size of anode powder. The line broadening method was employed to measure the crystallite size of NiO/10Sc1CeSZ powder according to Debye-Scherrer's method as follows [22]:

$$d_{\text{XRD}} = \frac{0.89\lambda}{\beta \cos\theta} \quad (1)$$

where λ and θ are the wavelength of Cu-K α radiation and Bragg angle, respectively. β represents the calibrated full width at half maximum (FWHM) of the (0 0 2) and (1 1 1) peaks for NiO and 10Sc1CeSZ powders, respectively (in radian). The microstructure of the calcined anode powder was observed with a transmission electron microscopy (TEM) system (Talos L120C, FEI, USA). The composition of elements in the calcined anode powder was estimated and confirmed close to the theoretically calculated composition by performing the energy dispersive spectroscopy (EDS; Merlin, Zeiss, Germany) and analyzing the results. The particle size distribution of calcined anode powder was analyzed by a laser scattering technique (Zetasizer Nanoseries, Malvern Instrument, UK).

Fabrication of symmetrical cells

NiO/10CeScZr|10ScCeZr|NiO-10ScCeZr symmetrical cells with 10Sc1CeSZ as an electrolyte were fabricated for electrochemical characterization. 10ScCeSZ electrolyte powder has been previously synthesized by a similar synthesis method of MW-GNP [22]. 10Sc1CeSZ electrolyte pellets were prepared by cold pressing into cylindrical pellets (diameter = 25 mm) using a uniaxial die press followed by sintering at 1400 °C in air for 5 h [22]. The sintered electrolyte pellets were polished with sandpapers to reduce the electrolyte thickness to approximately 1 mm, to obtain a smooth surface for good adherence, and to reduce the contact resistance between anode and electrolyte. The calcined NiO/10Sc1CeSZ anode powder was mixed with 2 wt% Hypermer KD15 solution as a dispersant (in acetone as a solvent) and was ball milled for 5 h using a zirconia (ZrO₂) jar and balls [33]. The ratio of anode powder to ZrO₂ balls (diameter = 5 mm) in weight was 1:4, and 250 rpm was set for the rotation speed of ball mill machine. The evaporation process of solvent in the mixture of anode

powder was conducted at 90 °C for 6 h in a drying oven. Then, the dried powder was thoroughly mixed in a solution of ink vehicle and homogenized by milling the mixture using a three-roll mill (EGM-65, ELE, China) for 30 min. The ink vehicle was made by mixing ethyl cellulose (binder, 2 wt% amount) and terpineol (solvent). The prepared anode ink was screen printed onto 10Sc1CeSZ pellet surface by a dry-and-paste method for 5 times on each side of the pellet to obtain sufficient thickness of anode layer. Then, the samples were sintered at 1300 °C for 4 h, and a symmetrical cell of NiO/10Sc1CeSZ|10Sc1CeSZ|NiO/10Sc1CeSZ was produced for the measurement. The active working area of the prepared symmetrical cell was 1 cm². It is based on the geometrical area of the circular-shaped screen-printed anode film. The anode film was reduced in humidified gas mixture of hydrogen and nitrogen (97 vol% H₂/N₂ (H₂:N₂ volume ratio = 10:90)–3 vol% H₂O) at 800 °C for 2 h to allow NiO to be fully reduced to Ni metal prior to the electrochemical impedance measurement. Scanning electron microscopy (SEM) images of the sample were captured through a SEM instrument (SU1510, Hitachi, Japan) to examine the microstructure of sintered anode film before and after reduction. The surface porosity of the reduced cermet anode film was evaluated using ImageJ software (Version 1.52g).

Electrical conductivity measurement

The direct-current (DC) conductivity of the reduced cermet anode pellet was measured through a four-point van der Pauw technique [34, 35] from 400 to 800 °C in a dry gas mixture of hydrogen and nitrogen atmosphere (H₂:N₂ volume ratio = 10:90). Pt wires were used as the four electrodes or probes. An electrical current source ($I = 100$ mA) was applied using a power supply (Keithley 2400) between probes 3 and 4. The output voltage values between probes 1 and 2, V_{12} (mV), were read several times and averaged to calculate the resistance, R_{12} ($=V_{12}/I$). The process of applying current and reading output voltage was repeated to obtain three other resistance values R_{23} , R_{34} , and R_{41} . The average of the four resistance values, R_{ave} (Ω), sheet resistance, R_s (Ω), and DC electrical conductivity, σ_{DC} (S/cm) was calculated using the following equations:

$$R_{\text{ave}} = (R_{12} + R_{23} + R_{34} + R_{41})/4 \quad (2)$$

$$R_s = (\pi/\ln 2) \cdot (R_{\text{ave}}) \quad (3)$$

$$\sigma_{\text{DC}} = 1/R_s l \quad (4)$$

where l is the sample thickness (in centimeter).

Electrochemical impedance measurement

The alternating-current (AC) electrochemical impedance of the prepared symmetrical cell was measured in a dry low hydrogen concentration atmosphere ($\text{H}_2:\text{N}_2$ volume ratio = 10:90), and a dry methane ($\text{CH}_4:\text{N}_2$ volume ratio = 50:50) at 600 and 800 °C. Autolab PGSTAT302N (Autolab 302, Eco Chemie, Netherlands) combined with a frequency response analyzer was used to conduct the AC electrochemical impedance measurement [35]. The measurements were conducted in potentiostatic mode over the frequency range of 0.01 Hz to 1 MHz at a sinusoidal voltage of 20 mV at the open-circuit voltage of the cell (0 V). The measurement results in the form of AC impedance spectra were plotted for the symmetrical cell. The plot known as Nyquist plot was plotted in Z real versus $-Z$ imaginary and the software of NOVA 1.11 was used in the analysis of electrochemical impedance (EIS) spectra.

Carbon deposition behavior of Ni/10Sc1CeSZ

The calcined NiO/10Sc1CeSZ anode powder was coarsened by subjecting to an additional heat treatment at 1300 °C for 4 h to evaluate carbon deposition onto the cermet material. One hundred milligrams of the coarse NiO/10Sc1CeSZ powder was then placed on pieces of quartz wool in a quartz tube fixed-bed reactor. The coarse NiO/10Sc1CeSZ powder was reduced for 2 h in humidified hydrogen gas (97 vol% H_2/N_2 ($\text{H}_2:\text{N}_2$ volume ratio = 10:90)–3 vol% H_2O) at 800 °C and exposed to a flow of dry methane gas ($\text{CH}_4:\text{N}_2$ volume ratio = 50:50) at 800 °C for 3 h. The total flow rate of the gas mixture was 100 mL/min. After that, laser Raman spectroscopy and thermogravimetric analysis (TGA) of the cermet powder were performed via a micro-Raman spectrometer (DXR2xi, Thermo Scientific, USA) with an excitation source from a laser operating at a wavelength of 532 nm and a thermogravimetric analyzer (TGA/DSC 1 HT, Mettler Toledo, USA) with a sensitivity of 0.0001 mg, respectively. TGA was conducted in air from 30 to 900 °C at a heating rate of 20 °C/min for the re-oxidation of carbon, which was deposited onto the cermet anode powder.

Results and discussion

Characterization of NiO/10Sc1CeSZ powder

The phase of NiO/10Sc1CeSZ powder synthesized by MW-GNP was determined by XRD. The phase analysis of XRD pattern and Rietveld refinement of the NiO/10Sc1CeSZ powder are shown in Fig. 1. The analysis of the XRD pattern by search and match revealed two phases of 10Sc1CeSZ phase and NiO phase having a cubic structure with Fm-3m space group. The phase identification was performed by using XRD

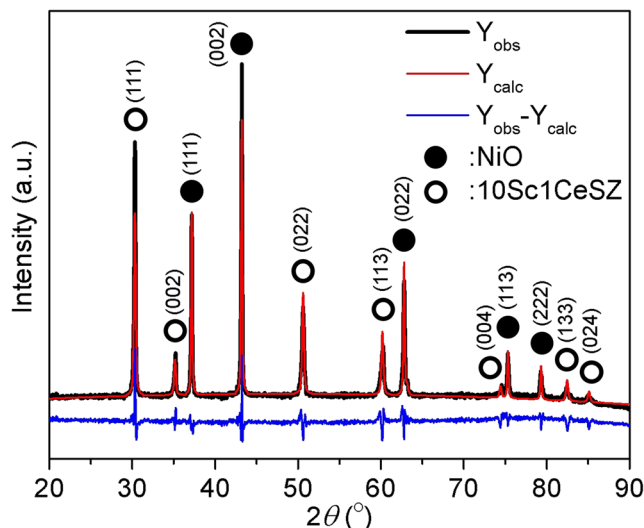
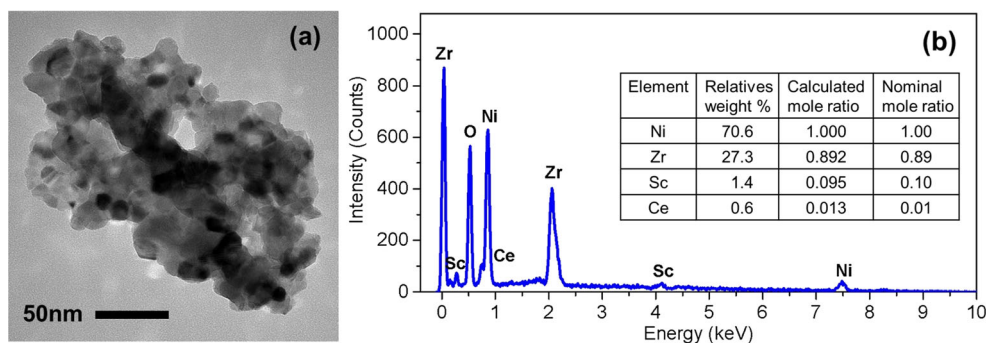


Fig. 1 XRD pattern of NiO/10Sc1CeSZ powder calcined at 800 °C in air for 2 h

reference patterns of ZrO_2 (XRD file number: 96–500-0039) and NiO (XRD file number: 96-101-0382). Impurities and other phases were not observed in the XRD data analysis which proved that the purity of the synthesized powder is high. In addition, the Rietveld refinement was conducted to further analyze the structure of the powders via X'Pert HighScore software. The powder exhibited a structure of cubic fluorite-type symmetry (Fm-3m space group) based on the Rietveld analysis and supported the result obtained from the analysis of XRD pattern. Based on the Rietveld refinement result, the final R goodness factors were $R_p = 7.114$, $R_{wp} = 9.4$, $R_e = 7.1$, and $\chi^2 = 1.753$, respectively. The successful refinement of the XRD data was indicated by the low value of χ^2 . The lattice parameter of the NiO phase was 4.1778 Å and that of the 10Sc1CeSZ phase was 5.0905 Å. The crystallite size calculated from Rietveld analysis using the Debye-Scherrer method [22] was 72.6 and 42.5 nm for the NiO and 10Sc1CeSZ phases, respectively. This measured crystallite size was considerably smaller than that of commercial NiO and 10Sc1CeSZ powders [10]. The small nickel particle size may enhance the catalytic activity by providing a large surface area of nickel cermet for fuel oxidation.

Figure 2a shows the TEM image of the calcined anode powder. The observed particle size of powder was within the range of 30–60 nm and in consistent with the XRD result. The image of powder captured by TEM clearly showed porous spongy-like and well-bonded particles. Some aggregation/agglomeration of particles was also observed, which may have affected the electrical properties and catalytic activity of cermet anode. Thus, the microwave-assisted solution combustion produced a cermet powder with nanosized particles that tended to bond together and form strong agglomerates. The EDS spectra of NiO/10Sc1CeSZ powder are presented in Fig. 2b, and the peaks of Ni, Sc, Ce, and Zr can be observed. Other

Fig. 2 **a** The morphology of calcined NiO/10Sc1CeSZ anode powder measured by TEM. **b** The elemental analysis of the powder by EDS



impurities including carbonaceous material were undetected in the calcined NiO/10Sc1CeSZ powder. The chemical composition of the anode powder was calculated using the relative weight percentage of the elements obtained from the EDS spectra. The chemical composition of the anode powder determined by EDS is comparable with the nominal composition of the powder as presented in Fig. 2b. These results showed that highly pure NiO/10Sc1CeSZ powder with two phases can be produced at the 800 °C calcination temperature.

Figure 3 presents the particle size distribution of NiO/10Sc1CeSZ anode powder synthesized by MW-GNP in comparison with the distribution of anode powders synthesized by other conventional methods. All the powders showed a similar bimodal distribution. However, the distribution of anode powder synthesized by MW-GNP is narrower than that synthesized by conventional methods. The distribution clearly indicates that the anode powder synthesized by MW-GNP is finer than the conventionally synthesized anode powders [7, 10, 36]. The synthesized NiO/10Sc1CeSZ powder is composed of fine particles (0.1–0.25 μm) and a small fraction of coarse particles (0.25–1.0 μm). This revealed that the MW-GNP is a very promising method to produce a homogeneous and uniform nanosized anode powder. The properties of anode powders synthesized by several conventional methods are summarized in Table 1.

Characterization of NiO/10Sc1CeSZ anode film

The SEM images of NiO/10Sc1CeSZ anode film surface after sintering at 1300 °C for 4 h in air and after reduction in

humidified gas mixture of hydrogen and nitrogen (97 vol% H₂/N₂ (H₂:N₂ volume ratio = 10:90)–3 vol% H₂O) gas at 800 °C for 2 h are shown in Figs. 4a and 4b, respectively. Both surface images exhibited particles connected to one another with < 1-μm particle sizes. The surface porosities estimated using ImageJ software for the anode film before and after reduction were 19.9% ± 0.1% and 33.3% ± 0.6%, respectively. The surface porosity of the anode film increased after it was reduced, reflecting the reduction of NiO to Ni. The estimated surface porosity is within the acceptable range (20–40%), and this value has significant impact on the electrochemical performance of the anode. Sufficient porosity is very critical for the diffusion of gas to the electrochemical reaction sites [1, 3, 9]. The cross-sectional image of the reduced Ni/10Sc1CeSZ anode film is shown in Fig. 4c. The average thickness of the reduced anode was approximately 15 μm. The image revealed the microstructure of anode having sufficient porosity at the interfacial region of anode-electrolyte as well as at the surface for the diffusion or transportation of gas to the electrochemical active sites and no delamination of anode coating film. The thickness should not exceed 35 μm to obtain low polarization resistance because the increase in thickness of anode coating may lead to difficulty in the transportation of gas to the electrochemical active sites [41].

Electrical conductivity of Ni/10Sc1CeSZ anode

The DC electrical conductivity, σ_{DC} of the Ni/10Sc1CeSZ cermet anode, as shown in Fig. 5, was about 580 S/cm at 700 °C operating temperature, which meets the electrical

Fig. 3 The particle size distribution of various anode powders [7, 10, 36]

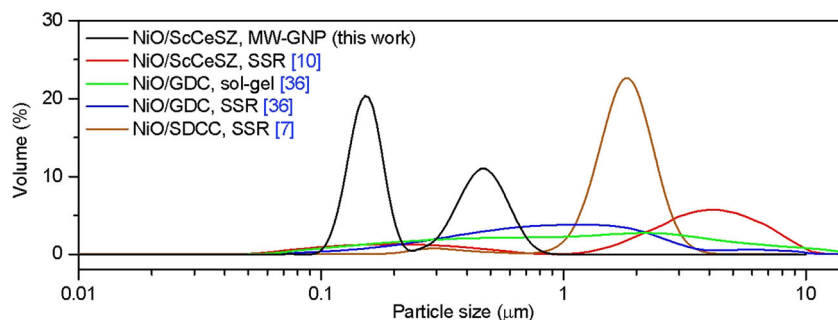


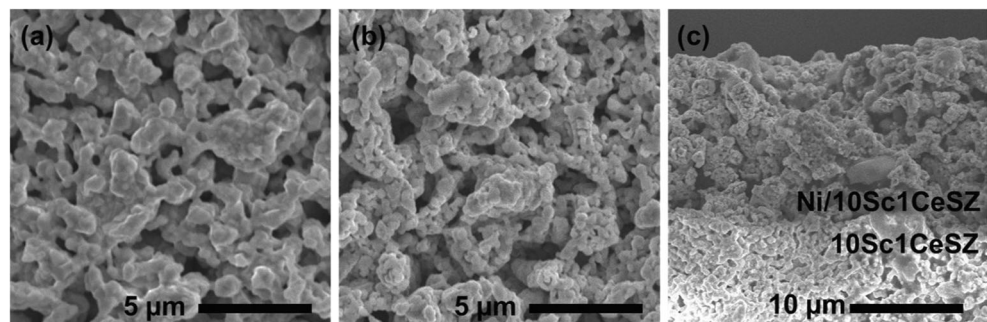
Table 1 Comparison of anode powder properties synthesized by different methods

Anode powder	Synthesis method	Powder properties	References
NiO/10Sc1CeSZ (50 vol% Ni)	MW-GNP	Crystallite size of 72.6 nm and 42.5 nm for NiO and 10Sc1CeSZ, respectively (XRD) Particle size in the range of 30–60 nm (TEM) Average particle size of 0.55 μm (particle size distribution) A high fraction of particle size in the range of 0.1–0.25 μm (particle size distribution) Bimodal and narrow particle size distribution	This work
NiO/10Sc1CeSZ (10–60 vol% Ni)	SSR	Average particle size in the range of 3.1–3.7 μm (particle size distribution) Bimodal and broad particle size distribution	[10]
NiO/ScSZ (80 wt% NiO)	SSR	Average particle size of 3.0 μm for NiO (SEM)	[37]
NiO/ScSZ (80 wt% NiO)	Co-precipitation	Average particle size of 0.3 μm for NiO (SEM)	[37]
NiO/YSZ (50 wt% NiO)	Co-precipitation	Average particle size of 0.3 μm (SEM)	[38]
NiO/YSZ (65 wt% NiO)	Two-step hydrothermal	Average particle size in the range of 0.05–0.1 μm for NiO and 0.2–0.3 μm for YSZ (XRD, FESEM, and TEM)	[39]
NiO/YSZ (60 wt% NiO)	SSR	Average particle size of 0.17 μm within the range of 0.06–0.5 μm (Particle size distribution) Monomodal and broad particle size distribution	[40]
NiO/GDC (50 wt% NiO)	SSR	Nanosized GDC and coarser NiO particles (SEM-EDS) A high fraction of particle size within the range of 0.1–3.0 μm (particle size distribution) Bimodal and broad particle size distribution	[36]
NiO/GDC (50 wt% NiO)	Sol-gel	Average particle size of less than 1.0 μm (SEM) A high fraction of particle size with less than 0.2 μm (particle size distribution)	[36]
NiO/SDCC (60 wt% NiO)	SSR	Bimodal and broad particle size distribution Average particle size in the range of 0.1–5.0 μm (particle size distribution) Bimodal and broad particle size distribution	[7]

conductivity value required of an anode material (≥ 100 S/cm) for SOFC applications. As expected, Ni/10Sc1CeSZ exhibited metallic conductivity, as its conductivity decreased with increased temperature. DC conductivity increased with decreased surface porosity, which has been previously reported (i.e., Ni/10Sc1CeSZ cermet exhibited a DC conductivity of around 1000 S/cm at 700 °C [10]). Ni-impregnated-ScSZ anodes have also shown a conductivity of 1010 S/cm, which decreases to 700 S/cm after 1000 min of operation in hydrogen fuel at 800 °C [42]. Ni/ScSZ prepared by solid-state

reaction further exhibits a conductivity of 250 S/cm at 900 °C, revealing that the size ratio between the larger sized NiO and the smaller sized ScSZ nanoparticle may affect the conductivity, leading to some NiO particles being covered by smaller ScSZ particles [43]. Some aggregation/agglomeration of particles about 2–3 μm in size was observed from the surface images of anode film. As a result, the porosity of cermet anode can be increased, which may decrease the contact networks of nickel–nickel particles and hence lead to lower conductivity. The conductivities of anodes shown in Fig. 5 are

Fig. 4 Surface SEM image of **a** NiO/10Sc1CeSZ anode film sintered at 1300 °C and **b** Ni/10Sc1CeSZ anode film reduced in humidified gas mixture of hydrogen and nitrogen (97 vol% H₂/N₂ ((H₂:N₂ volume ratio = 10:90)–3 vol% H₂O) at 800 °C. **c** Cross-sectional SEM images of the reduced Ni/10Sc1CeSZ anode film.



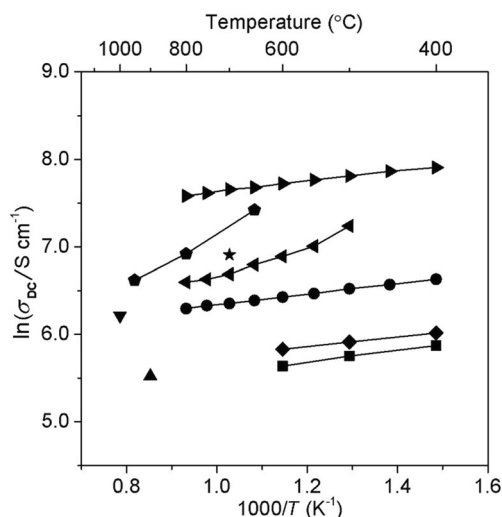


Fig. 5 DC electrical conductivity of various nickel cermet anodes (Ni/10Sc1CeSZ, Ni/ScSZ, Ni/YSZ, Ni/SDC, and Ni/GDC) as a function of temperature measured in dry H₂ atmosphere. Black circle indicates Ni/10Sc1CeSZ (Ni = 50 vol%; sintered at 1300 °C for 4 h)—this work; right-pointed black triangle indicates Ni/10Sc1CeSZ (Ni = 50 vol%; sintered at 1350 °C for 1 h)—solid-state reaction [10]; black star indicates Ni/10Sc1CeSZ (Ni = 40 vol%; sintered at 1300 °C for 1 h)—solid-state reaction [10]; black pentagon indicates Ni/ScSZ (Ni = 40 wt%; impregnated nickel(II) nitrate was decomposed at 550 °C for 1 h, 12 impregnation cycles)—impregnation method [42]; black up-pointed triangle indicates Ni/ScSZ (Ni = 50 vol%; sintered at 1200 °C for 4 h)—solid-state reaction [43]; black down-pointed triangle represents Ni/YSZ (Ni = 50 vol%)—solid-state reaction [3], (black left-pointed triangle represents Ni/SDC (NiO = 65 wt%; sintered at 1300 °C for 4 h)—glycine nitrate process [21]; black diamond represents Ni/GDC (Ni = 50 vol%; sintered at 1300 °C for 2 h)—citrate nitrate process [18]; and (black square represents Ni/SDC (Ni = 50 vol%; sintered at 1300 °C for 2 h)—citrate nitrate process [18]

also closely related to the powder processing method, fabrication conditions (e.g., sintering temperature and time), Ni content, and characteristics of the synthesized anode powder. This can be a reason for different conductivities shown by the anodes shown in Fig. 5. Also, the figure indicated that Ni/10Sc1CeSZ powder synthesized by MW-GNP in this study showed an acceptable conductivity (> 100 S/cm) and is a potential processing method to produce powders with improved properties.

Electrochemical performance of Ni/10Sc1CeSZ anode

Figure 6 shows the electrochemical impedance spectra (EIS) of a symmetrical cell consisting of Ni/10Sc1CeSZ cermet anode operated at 800 °C under dry low hydrogen concentration (H₂:N₂ = 10:90) and dry methane (CH₄:N₂ = 50:50) fuels, respectively. The fitting process of the AC impedance plots was performed according to the equivalent electrical circuit consisting resistance (*R*) and constant phase element (CPE) as shown in the inset of Fig. 6, in which the resistances and constant phase elements are illustrated by *R_s*, *R₁*, *R₂*, CPE₁, and CPE₂, respectively. Two semicircles were observed from

the EIS spectra, and they represent the middle- and low-frequency regions related to the reaction on the anode surface and at the interfacial region of anode-electrolyte. As shown in Fig. 6, the relaxation frequency was about 1200 Hz at the middle region and 6 Hz at the low region under H₂ (10 vol%) atmosphere. Meanwhile, the relaxation frequency at the middle and low region under dry CH₄ (50 vol%) atmosphere was 290 Hz and 20 Hz, respectively. The total electrode polarization resistance, *R_p* (Ω), and area specific resistance (ASR) can be calculated from the impedance spectra of a symmetrical cell by the following equations:

$$R_p = R_1 + R_2 \tag{6}$$

$$ASR = R_p A / 2 \tag{7}$$

where *R₁* and *R₂* are the polarization resistances for the process of charge transfer and gas diffusion obtained from the impedance spectra. *A* is the active working area (1 cm²).

As expected, Ni/10Sc1CeSZ cermet anode operated in dry methane fuel exhibited a larger ASR value than that in dry hydrogen fuel in all operating temperatures. This is because the operation in methane fuel led to carbon deposition onto the cermet anode. The ASRs obtained at the operating temperature of 800 °C in dry low hydrogen concentration (10 vol%) and dry methane (50 vol%) fuels were found to be 0.96 and 24.3 Ω cm², respectively. The obtained electrochemical performance of Ni/10ScCeSZ anode in this study is acceptable because its performance was measured under dry low hydrogen concentration and dry methane fuels with electrolyte-supported symmetrical cells.

Table 2 shows the ASRs of the nickel cermet obtained from this work and nickel cermets from the literature with different

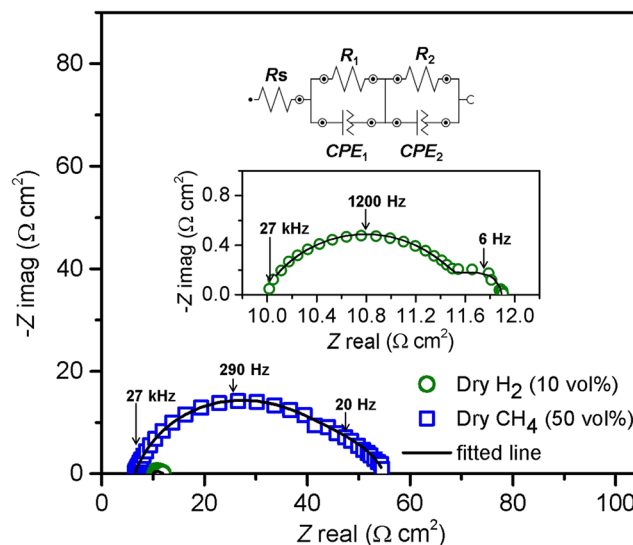


Fig. 6 AC impedance spectra of a symmetrical cell consisting of Ni/10Sc1CeSZ anode measured at 800 °C operating temperature in dry hydrogen (10 vol%) and methane (50 vol%) fuels

powder synthesis techniques, fuel concentrations, and cell designs at 800 °C. The Ni/10Sc1CeSZ anode with electrolyte-supported design in this study exhibited a reasonably lower ASR value even in low hydrogen concentration (10 vol%) fuel compared with the ASR values measured with Ni/10Sc1CeSZ anode synthesized by the SSR method and other types of nickel cermet anodes (Ni/GDC, Ni/YSZ, and Ni/SDC) as shown in Table 2. A comparable ASR measured under humidified low hydrogen concentration fuel (2% H₂–95% Ar–3% H₂O) was found for Ni/10Sc1CeSZ cermet anode prepared by SSR as shown in Table 2. However, the electrolyte thickness (0.2 mm) of the symmetrical cell was thinner than the electrolyte fabricated in this work (1.0 mm) for the preparation of electrolyte-supported symmetrical cells. The ASR of Ni/YSZ operated in hydrogen fuel was obtained using a symmetrical

cell with anode-supported design [46] and seemed comparable with the ASRs for the Ni/10Sc1CeSZ cermet obtained from electrolyte-supported design in the present work. Cell fabrication using different designs such as anode-supported, cathode-supported, and electrolyte-supported types can also significantly affect the ASR of nickel cermet anode. A symmetrical cell prepared with an anode-supported design contains a thin electrolyte layer sandwiched between two thick anode layers, which improves the electrochemical process, reduces polarization loss, and increases the cell performance [50–52]. The material properties and design adopted in cell fabrication (symmetrical or single cell) are very critical to enhance the performance of electrodes or cells. Thus, the improved electrochemical performance of the cermet anode even at low hydrogen concentration in this study can be related to

Table 2 ASRs of various nickel cermet anodes in hydrogen and methane fuels using a symmetrical cell measured at 800 °C

Cermet anode (Ni content)	Synthesis method (sintering conditions)	Cell design	Fuels (vol%)	Steam-to-carbon ratio	ASR (Ω cm ²)	References
Ni/10Sc1CeSZ (50 vol% Ni)	Microwave-assisted glycine nitrate process, MW-GNP (1300 °C, 4 h)	Electrolyte-supported	10% H ₂ –90% N ₂	–	0.96	This work
Ni/10Sc1CeSZ (50 vol% Ni)	MW-GNP (1300 °C, 4 h)	Electrolyte-supported	50% CH ₄ –50%N ₂	Dry CH ₄	24.3	This work
Ni/10Sc1CeSZ (40 vol% Ni)	Solid-state reaction, SSR (1300 °C, 1 h)	Electrolyte-supported	49% H ₂ –48%N ₂ –3% H ₂ O	–	1.8	[10]
Ni/10Sc1CeSZ (40 vol% Ni)	Solid-state reaction, SSR (1300 °C, 1 h)	Electrolyte-supported	97% H ₂ –3% H ₂ O	–	0.75	[44]
Ni/10Sc1CeSZ (60 vol% NiO)	SSR (1300 °C, 3 h)	Electrolyte-supported	2% H ₂ –95% Ar–3% H ₂ O	–	0.95	[41]
Ni/YSZ (60 vol% Ni)	Solid liquid method, SLM (1500 °C, 1 h)	Electrolyte-supported	CH ₄ –5% H ₂ O	0.05	45	[45]
Ni/YSZ (34 vol% Ni)	SSR (1350 °C, 3 h)	Anode-supported	CH ₄ –45% H ₂ O	0.80	18	[46]
Ni/YSZ (60 wt% NiO)	SSR (1300 °C)	Electrolyte-supported	97% H ₂ –3% H ₂ O	–	1.33	[46]
Ni/YSZ (60 wt% NiO)	SSR (1300 °C)	Electrolyte-supported	15% H ₂ –82.5% N ₂ –2.5% H ₂ O	–	7.0 ^a	[47]
Ni/YSZ (60 wt% NiO)	SSR (1300 °C)	Electrolyte-supported	15% H ₂ –85% N ₂ –benzene (C ₆ H ₆ , as model tar, 15 g m ^{–3})	Dry H ₂ /C ₆ H ₆	240 ^a	[47]
Ni/YSZ (60 wt% NiO)	SSR (1300 °C)	Electrolyte-supported	15% H ₂ –82.5% N ₂ –2.5% H ₂ O–C ₆ H ₆ model tar	1.0	19 ^a	[47]
Ni/GDC (60 vol% Ni)	GNP (1200 °C, 2 h)	Electrolyte-supported	100% H ₂	–	9.8	[19]
Ni/GDC (60 vol% Ni)	GNP (1200 °C, 2 h)	Electrolyte-supported	100% CH ₄	Dry CH ₄	1994	[19]
Ni/GDC (50 wt% NiO)	SSR (1300 °C)	Electrolyte-supported	15% H ₂ –82.5% N ₂ –2.5% H ₂ O	–	1.04	[47]
Ni/GDC (50 wt% NiO)	SSR (1300 °C)	Electrolyte-supported	15% H ₂ –82.5% N ₂ –2.5% H ₂ O–C ₆ H ₆ model tar	1.0	1.0 ^a	[47]
Ni/GDC (50 wt% NiO)	SSR (1300 °C)	Electrolyte-supported	15% H ₂ –80% N ₂ –5% H ₂ O–C ₆ H ₆ model tar	2.0	1.1 ^a	[47]
Ni/GDC (50 wt% NiO)	SSR (1300 °C, 2 h)	Electrolyte-supported	15% H ₂ –77.5% N ₂ –7.5% H ₂ O–C ₆ H ₆ model tar	3.0	1.34 ^a	[47]
Ni/SDC (55 wt% NiO)	GNP–SSR (1330 °C, 5 h)	Anode-supported	97% H ₂ –3% H ₂ O	–	0.058 ^b	[4]
Ni/SDC (55 wt% NiO)	GNP–SSR (1330 °C, 5 h)	Anode-supported	100% CH ₄	Dry CH ₄	0.104 ^c	[4]
Ni/SDC (70 wt% NiO)	SSR (microwave sintering, 1200 °C, 1 h)	Anode-supported	97% H ₂ –3% H ₂ O	–	4.5	[48]
Ni/SDC (70 wt% NiO)	SSR (conventional sintering, 1200 °C, 1 h)	Anode-supported	97% H ₂ –3% H ₂ O	–	7.5	[48]
Ni/SDC (55 wt% NiO)	GNP–SSR (1330 °C, 5 h)	Anode-supported	97% H ₂ –3% H ₂ O	–	0.58 ^d	[49]
Ni/SDC (55 wt% NiO)	GNP–SSR (1330 °C, 5 h)	Anode-supported	40% CO–60%CO ₂	Dry CO/CO ₂	0.6 ^d	[49]

^a An electrolyte-supported cell measured at 765 °C (current density = 0 A cm^{–2})

^b An anode-supported cell measured at 700 °C (current density = 0.35 A cm^{–2})

^c An anode-supported cell measured at 700 °C (current density = 0.35 A cm^{–2} and 100-h operation)

^d An anode-supported cell measured at 550 °C (current density = 0.1 A cm^{–2})

the improved morphology of the synthesized powder using the uniform heating source of microwave energy as confirmed from Fig. 3.

The operation conditions such as hydrogen concentration and humidity in fuel supply can also affect the performance of the anodes. For instance, the ASR value of Ni/10Sc1CeSZ at 800 °C was 0.75 Ω cm² and 1.8 Ω cm² measured in 97% H₂–3% H₂O [44] and 49% H₂–48% N₂–3% H₂O [10], respectively. However, the ASR value of Ni/10Sc1CeSZ anode measured in low hydrogen concentration fuel and dry condition seems better than the reported literature values shown in Table 2.

The ASR value of Ni/10Sc1CeSZ cermet anode operated in methane fuel was higher than that in hydrogen fuel due to the deposition of carbon onto the anode surface. However, the value was less than that for other types of nickel cermet anodes (e.g., Ni/YSZ and Ni/GDC) under the similar condition as shown in Table 2. This result is in consistent with the improved electrochemical performance of the anode even at low hydrogen concentration in this study. Anode polarization resistance also reportedly decreases with decreased methane fuel volume and increased steam-to-carbon ratio [13, 45]. Even though dry methane reforming by the cermet anode was the focus of this work, the existence of steam will help remove carbon on the anode surface and increase the active sites for the electrocatalytic reaction of cermet toward methane fuel, thereby enhancing the anode performance.

The results obtained from this study suggested that the preparation of Ni/10Sc1CeSZ anode by MW-GNP improved the morphology of the anode material. Furthermore, the modification of the cermet anode and operating condition should be further improved to achieve the high electrochemical performance required for SOFC anode materials, particularly when using hydrocarbon fuel.

Based on the obtained ASRs, the Arrhenius plots for the symmetrical cell consisting of Ni/10Sc1CeSZ anode operated under dry low hydrogen concentration (10 vol%) and dry methane (50 vol%) fuels between 600 and 800 °C are shown in Fig. 7. The Arrhenius plots were obtained by plotting $\ln(\text{ASR})$ versus $1000/T$. Based on the Arrhenius equation, the activation energy, E_a (eV), was evaluated using the slope value of the fitted line. The Arrhenius equation is expressed in Eq. (6) as follows:

$$\ln(\text{ASR}) = -(E_a/k) \cdot (1/T) + \ln A \quad (6)$$

where A , T , and k are the pre-exponential factor, the absolute temperature (K), and the Boltzmann's constant (8.617×10^{-5} eV/K), respectively. The activation energy, E_a , of the cermet in dry hydrogen (10 vol%) and dry methane (50 vol%) fuels obtained from the linear fit of plots was 1.052 ± 0.027 and 1.069 ± 0.029 eV, respectively. The E_a

was close to one another for dry hydrogen (10 vol%) and dry methane (50 vol%) fuels, indicating that a similar process occurred in both atmospheres at intermediate operating temperatures (600–800 °C). This value may be assigned to electrochemical oxidation of fuels related to Ni particle size.

Carbon deposition behavior of Ni/10Sc1CeSZ

Carbon deposition behavior is one of the important criteria for SOFC anode component under application in hydrocarbon fuel. The amount of carbon deposited onto Ni/10Sc1CeSZ cermet anode powder can be estimated from the thermogravimetric analysis (TGA) result as shown in Fig. 8. The weight loss between 500 and 700 °C was due to the re-oxidation of deposited carbon by oxygen [19, 55]. In this study, the weight loss due to re-oxidation of carbon was 4.34%. This carbon deposition onto the cermet anode after treatment in dry methane atmosphere is expected to occur through the methane pyrolysis ($\text{CH}_4 \rightarrow \text{C} + 2\text{H}_2$).

The amount of carbon deposited onto the anode synthesized by MW-GNP in this study was lower compared with that deposited onto the similar anode synthesized by solid-state reaction (ca. 15%) and co-precipitation (ca. 45%) methods [37]. Based on TGA results in Fig. 8, it is further confirmed that anode synthesized by MW-GNP in this study

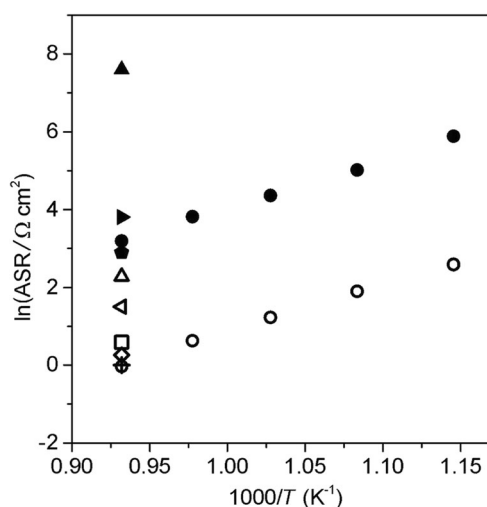


Fig. 7 Arrhenius plots of the area specific resistance for various nickel cermet anodes in H₂ and CH₄ fuel. H₂: white circle represents Ni/10Sc1CeSZ—this work, $E_a = 1.05$ eV; white square represents Ni/10Sc1CeSZ—solid-state reaction [10]; + represents Ni/10Sc1CeSZ—solid-state reaction [41]; white diamond represents Ni/YSZ—solid-state reaction [46]; white up-pointed triangle represents Ni/GDC—glycine nitrate process [19]; and white left-pointed triangle represents Ni/SDC—solid-state reaction [48]. CH₄: black circle represents Ni/10Sc1CeSZ—this work, $E_a = 1.07$ eV; black up-pointed triangle represents Ni/GDC—glycine nitrate process [19]; black right-pointed triangle represents Ni/YSZ—solid-liquid method (steam-to-carbon ratio = 0.05) [45]; and black pentagon represents Ni/YSZ—solid-liquid method (steam-to-carbon ratio = 0.75) [45]

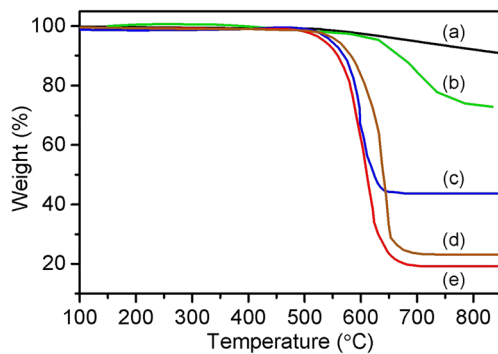


Fig. 8 Thermogravimetric result of various cermet powders after treatment in methane atmosphere. (a) Ni/10Sc1CeSZ cermet powder in dry methane atmosphere at 800 °C for 3 h (this work). (b) Ni/ScSZ in humidified methane atmosphere at 600 °C for 2 h [53]. (c) Ni/Al₂O₃. (d) Ni/TiO₂(15%)–Al₂O₃. (e) Ni/TiO₂(50%)–Al₂O₃ in dry methane atmosphere at 700 °C for 6.5 h [54]

exhibited a low amount of deposited carbon onto anode as compared with anodes synthesized by other methods such as solid-state reaction and co-precipitation [53, 54]. The carbon deposition onto the anode is dependent on the surface area and particle size of the synthesized anode powders. Generally, an anode powder with smaller NiO particle size tends to accumulate higher amount of carbon on the surface of the powder. Particle size for the anode material prepared in this study was around 2–3 μm as compared with that synthesized by solid-state reaction and co-precipitation methods which were 3 μm and 0.3 μm, respectively [37]. This explained why the amount of carbon deposited on the anode powder synthesized by this study is considerably low. The higher amount of carbon accumulated on the active site of an anode may decrease the lifetime and performance of the anode. It can be said that the carbon deposition problem in an anode is mainly dependent on the particle size of NiO and in agreement with other reported studies [2, 37]. Therefore, an appropriate range of NiO particle size needs to be considered during the fabrication stage to minimize the amount of carbon deposited onto the Ni-based anodes.

Figure 9 shows the Raman spectra of the Ni/10Sc1CeSZ cermet after treatment in dry methane gas at 800 °C for 3 h. The structure of carbon formed on the cermet was determined from Raman spectra. The defect (D), graphite (G), and 2D bands of carbon were observed through three peaks at the Raman shifts of 1342, 1563, and 2667 cm⁻¹, respectively. The graphitization degree of carbon is usually assigned by the intensity ratio of G-band peak to D-band peak (peak intensity ratio of G/D or I_G/I_D) calculated from the Raman spectra [14, 56]. G-band and D-band corresponded to crystalline graphite and amorphous carbon. The I_G/I_D for the cermet anode after treatment in dry methane gas was 2.1 as calculated from the Raman spectra.

The graphitization degree of anode prepared by MW-GNP in this study was higher than that prepared by solid-state

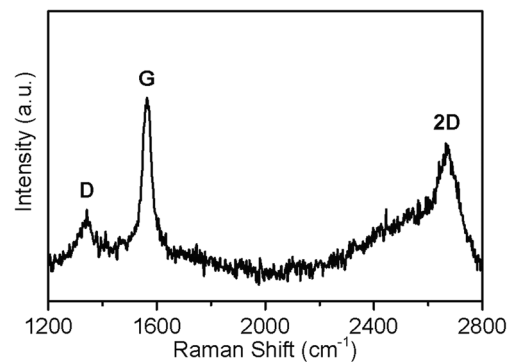


Fig. 9 Raman spectra of Ni/10Sc1CeSZ cermet powder after treatment in dry methane atmosphere at 800 °C for 3 h

reaction which was in the range of 1.1–1.4 after exposure between 600 and 1000 °C for 1 h [53]. However, the highest graphitization degree was reported as 10 for Ni/ScSZ anode prepared by co-precipitation method after exposure at 1000 °C for 1 h [37]. The graphitization degree of an anode is affected by the particle size of Ni, exposure temperature, and time. The lower value of I_G/I_D indicates the higher formation of amorphous carbon structure that can deteriorate the characteristics of anode toward dry methane fuel and may decrease the performance of SOFC. Although the graphitization value of the anode prepared by MW-GNP method in this study is lower than that prepared by co-precipitation method [37], the amount of carbon deposited onto the anode was considerably low. This result also confirmed that the catalytic activity of Ni/10Sc1CeSZ cermet anode operated in dry methane was suppressed by the formation of amorphous carbon.

Conclusion

NiO/10Sc1CeSZ anode powder has been successfully synthesized by microwave-assisted glycine nitrate process (MW-GNP). The synthesized anode powder consisted of two phases of cubic NiO and cubic 10Sc1CeSZ with the crystallite sizes of 67 and 40 nm, respectively. The electrical conductivity of the anode at 800 °C was 580 S/cm, which is in the acceptable range (> 100 S/cm) and suitable for SOFC application. The measured surface porosity of the reduced anode was 33 vol% and also within the acceptable range (20–40 vol%). The electrochemical measurement of the reduced Ni/10Sc1CeSZ cermet anode using 10Sc1CeSZ electrolyte-supported symmetrical cells after 60 min of fuel utilization at 800 °C revealed that the ASRs were 0.96 and 24.3 Ω cm² in dry low hydrogen concentration (10 vol% hydrogen–90 vol% nitrogen) and dry methane (50 vol% methane–50 vol% nitrogen) fuels, respectively. The obtained ASR values especially at low hydrogen concentration were better than the ASR values other Ni-based anodes measured at humidified high hydrogen concentration and humidified methane fuels. The amount of carbon

deposited onto the prepared anode is only 4.34% after 3-h exposure in dry methane fuel at 800 °C. Overall, the improved performance of Ni/10Sc1CeSZ cermet anode in this study was due to the improved morphology of cermet powder synthesized by glycine nitrate process assisted by uniform microwave heating. This method can be considered a potential powder processing method in the preparation of high-performance SOFC materials.

Acknowledgments Abdul Azim Jais gratefully acknowledges the Ministry of Education Malaysia and Universiti Malaysia Pahang for the PhD scholarship. The authors thankfully acknowledge the Centre for Research and Instrumentation Management, Universiti Kebangsaan Malaysia, for providing excellent testing equipment.

Funding information This study was financially supported by Universiti Kebangsaan Malaysia and the Ministry of Higher Education via the grant of Research University (Grant number DIP-2018-013) and the Fundamental Research Grant Scheme (FRGS/2/2014/ST05/UKM/03/1), respectively.

References

- Shaikh SP, Muchtar A, Somalu MR (2015) A review on the selection of anode materials for solid-oxide fuel cells. *Renew Sust Energy Rev* 51:1–8
- Wang W, Su C, Wu Y, Ran R, Shao Z (2013) Progress in solid oxide fuel cells with nickel-based anodes operating on methane and related fuels. *Chem Rev* 113(10):8104–8151
- Prakash BS, Kumar SS, Aruna S (2014) Properties and development of Ni/YSZ as an anode material in solid oxide fuel cell: a review. *Renew Sust Energy Rev* 36:149–179
- Ideris A, Croiset E, Pritzker M, Amin A (2017) Direct-methane solid oxide fuel cell (SOFC) with Ni-SDC anode-supported cell. *Int J Hydrog Energy* 42(36):23118–23129
- Itagaki Y, Cui J, Ito N, Aono H, Yahiro H (2018) Electrophoretically deposited Ni-loaded (SmO_{1.5})_{0.2}(CeO₂)_{0.8} anode for ammonia-fueled solid oxide fuel cell. *ECS Trans* 85(13):779–786
- Chen Z-y, Bian L-z, Yu Z-y, Wang L-j, Li F-s, Chou K-C (2018) Effects of specific surface area of metallic nickel particles on carbon deposition kinetics. *Int J Miner Metall Mater* 25(2):226–235
- Mahmud LS, Muchtar A, Somalu MR (2016) Influence of sintering temperature on NiO-SDCC anode for low-temperature solid oxide fuel cells (LT-SOFCs). *Ceramics-Silikáty* 60(4):317–323
- Syednezhad M, Rajabi A, Muchtar A, Somalu MR (2016) Nanostructured and nonsymmetrical NiO-SDC/SDC composite anode performance via a microwave-assisted route for intermediate-temperature solid oxide fuel cells. *Mater Manuf Process* 31(10):1301–1305
- Ng KH, Rahman HA, Somalu MR (2018) Enhancement of composite anode materials for low-temperature solid oxide fuels. *Int J Hydrog Energy* 44:30692–30704
- Somalu MR, Yufit V, Cumming D, Lorente E, Brandon N (2011) Fabrication and characterization of Ni/ScSZ cermet anodes for IT-SOFCs. *Int J Hydrog Energy* 36(9):5557–5566
- Baity PSN, Budiana B, Suasmoro S (2017) Preparation of Ni-YSZ cermet through reduction of NiO-YSZ ceramic for SOFC anode. *IOP Conference Series: Mater Sci Eng* 214(1):012029
- Kim J, Cho K, Kagomiya I, Park K (2013) Structural studies of porous Ni/YSZ cermets fabricated by the solid-state reaction method. *Ceram Int* 39(7):7467–7474
- Bebelis S, Tiropani C, Neophytides S (2001) Polarization behavior of Ni-YSZ cermet anodes in YSZ fuel cells running on methane under internal reforming conditions. *Ionics* 7(1–2):32–43
- Hua B, Li M, Chi B, Jian L (2014) Enhanced electrochemical performance and carbon deposition resistance of Ni-YSZ anode of solid oxide fuel cells by in situ formed Ni-MnO layer for CH₄ on-cell reforming. *J Mater Chem A* 2(4):1150–1158
- Liu Z, Liu B, Ding D, Liu M, Chen F, Xia C (2013) Fabrication and modification of solid oxide fuel cell anodes via wet impregnation/infiltration technique. *J Power Sources* 237:243–259
- Connor PA, Yue X, Savaniu CD, Price R, Triantafyllou G, Cassidy M, Kerherve G, Payne DJ, Maher RC, Cohen LF (2018) Tailoring SOFC electrode microstructures for improved performance. *Advan Energy Mater* 8(23):1800120
- Zielke P, Xu Y, Simonsen SB, Norby P, Kiebach R (2016) Simulation, design and proof-of-concept of a two-stage continuous hydrothermal flow synthesis reactor for synthesis of functionalized nano-sized inorganic composite materials. *J Supercrit Fluids* 117:1–12
- Skalar T, Zupan K, Marinšek M (2019) Microstructure tailoring of combustion-derived Ni-GDC and Ni-SDC composites as anode materials for intermediate temperature solid oxide fuel cells. *J Aust Ceram Soc* 55(1):123–133
- Cho CK, Choi BH, Lee KT (2012) Effect of Co alloying on the electrochemical performance of Ni-Ce_{0.8}Gd_{0.2}O_{1.9} anodes for hydrocarbon-fueled solid oxide fuel cells. *J Alloys Compd* 541:433–439
- Garcia RM, Cervera RB (2019) Morphology and structure of Ni/Zr_{0.84}Sc_{0.16}O_{1.92} electrode material synthesized via glycine-nitrate combustion method for solid oxide electrochemical cell. *Appl Sci* 9(2):264–273
- Yang C, Cheng JG, He HG, Gao JF (2010) Ni/SDC materials for solid oxide fuel cell anode applications by the glycine-nitrate method. *Key Eng Mater* 434:731–734
- Jais AA, Muhammed Ali SA, Anwar M, Somalu MR, Muchtar A, Isahak WNRW, Tan CY, Singh R, Brandon NP (2017) Enhanced ionic conductivity of scandia-ceria-stabilized-zirconia (10Sc1CeSZ) electrolyte synthesized by the microwave-assisted glycine nitrate process. *Ceram Int* 43(11):8119–8125
- Ali SM, Anwar M, Somalu MR, Muchtar A (2017) Enhancement of the interfacial polarization resistance of La_{0.6}Sr_{0.4}Co_{0.2}Fe_{0.8}O_{3-δ} cathode by microwave-assisted combustion method. *Ceram Int* 43(5):4647–4654
- Ao H, Liu X, Zhang H, Zhou J, Huang X, Feng Z, Xu H (2015) Preparation of scandia stabilized zirconia powder using microwave-hydrothermal method. *J Rare Earths* 33(7):746–751
- Molero-Sánchez B, Prado-Gonjal J, Ávila-Brandé D, Birss V, Morán E (2015) Microwave-assisted synthesis and characterization of new cathodic material for solid oxide fuel cells: La_{0.3}Ca_{0.7}Fe_{0.7}Cr_{0.3}O_{3-δ}. *Ceram Int* 41(7):8411–8416
- Vijay SK, Chandramouli V, Khan S, Clinsha P, Anthonysamy S (2014) Microwave assisted gel-combustion synthesis of 8mol% YSZ: a study of the effect of fuel on the ionic conductivity. *Ceram Int* 40(10):16689–16699
- Tongxiang C, Yanwei Z, Wei Z, Cuijing G, Xiaowei Y (2010) Synthesis of nanocomposite nickel oxide/yttrium-stabilized zirconia (NiO/YSZ) powders for anodes of solid oxide fuel cells (SOFCs) via microwave-assisted complex-gel auto-combustion. *J Power Sources* 195(5):1308–1315
- Ramesh S, Zulkifli N, Tan CY, Wong YH, Tarlochan F, Teng WD, Sopyan I, Bang LT, Sarhan AAD (2018) Comparison between microwave and conventional sintering on the properties and

- microstructural evolution of tetragonal zirconia. *Ceram Int* 44(8): 8922–8927
29. Chandore V, Carpenter G, Sen R, Gupta N (2013) Synthesis of nano crystalline ZnO by microwave assisted combustion method: an eco friendly and solvent free route. *Int J Environ Sci: Dev Monit(IJESDM)* 4(2):45–47
 30. Garadkar K, Kadam A, Park J (2018) Microwave-assisted sol-gel synthesis of metal oxide nanomaterials. In: Klein L, Aparicio M, Jitianu A (eds) *Handbook of sol-gel science and technology*. Springer International Publishing, New York, pp 483–504
 31. Shaikh SP, Somalu MR, Muchtar A (2016) Nanostructured Cu-CGO anodes fabricated using a microwave-assisted glycine-nitrate process. *J Phys Chem Solids* 98:91–99
 32. Sun H, Zhang Y, Gong H, Li Q, Bu Y, Li T (2016) Anode-supported SOFCs based on $\text{Sm}_{0.2}\text{Ce}_{0.8}\text{O}_{2-\delta}$ electrolyte thin-films fabricated by co-pressing using microwave combustion synthesized powders. *Ceram Int* 42(3):4285–4289
 33. Somalu MR, Muchtar A, Daud WRW, Brandon NP (2017) Screen-printing inks for the fabrication of solid oxide fuel cell films: a review. *Renew Sust Energ Rev* 75:426–439
 34. Samat AA, Jais AA, Somalu MR, Osman N, Muchtar A, Lim KL (2018) Electrical and electrochemical characteristics of $\text{La}_{0.6}\text{Sr}_{0.4}\text{CoO}_{3-\delta}$ cathode materials synthesized by a modified citrate-EDTA sol-gel method assisted with activated carbon for proton-conducting solid oxide fuel cell application. *J Sol-Gel Sci Technol* 86(3):617–630
 35. Baharuddin NA, Muchtar A, Somalu MR, Kalib NS, Raduwan NF (2019) Synthesis and characterization of cobalt-free $\text{SrFe}_{0.8}\text{Ti}_{0.2}\text{O}_{3-\delta}$ cathode powders synthesized through combustion method for solid oxide fuel cells. *Int J Hydrog Energy* 44(58):30682–30691
 36. Macedo DA, Figueiredo FM, Paskocimas CA, Martinelli AE, Nascimento RM, Marques FM (2014) Ni-CGO cermet anodes from nanocomposite powders: microstructural and electrochemical assessment. *Ceram Int* 40(8):13105–13113
 37. Puengjinda P, Muroyama H, Matsui T, Kawano M, Inagaki T, Eguchi K (2010) Influence of preparation methods on the carbon deposition and reduction behavior of Ni-ScSZ cermet. *J Electrochem Soc* 157(11):B1673–B1678
 38. Yoshito WK, Ussui V, Lazar DRR, Pascoal JOA (2005) Synthesis and characterization of NiO-8YSZ powders by coprecipitation route. In: *Materials science forum*. Trans Tech Publ 498-499:612–617
 39. Kim B, Cho K, Choi J, Shin D (2015) Preparation of NiO-YSZ composite powder through 2-step hydrothermal synthesis and its application to solid oxide fuel cell anode functional layer. *J Nanosci Nanotechnol* 15(1):536–539
 40. Tanhaei M, Mozammel M, Javanshir E, Ilkhechi NN (2017) Porosity, microstructure and mechanical behavior of NiO-YSZ composite anode for solid oxide fuel cells. *Int J Mater Res* 108(10):857–863
 41. Patro P, Delahaye T, Bouyer E, Sinha P (2012) Microstructural development of Ni-1Ce10ScSZ cermet electrode for solid oxide electrolysis cell (SOEC) application. *Int J Hydrog Energy* 37(4): 3865–3873
 42. Chen J, Bertei A, Ruiz-Trejo E, Atkinson A, Brandon NP (2017) Characterization of degradation in nickel impregnated scandia-stabilize zirconia electrodes during isothermal annealing. *J Electrochem Soc* 164(9):F935–F943
 43. Spirin A, Nikonov A, Lipilin A, Khrustov V, Kuterbekov K, Nurakhmetov T, Bekmyrza KZ (2016) Effect of structural parameters of Ni-ScSZ cermet components on the SOFC anodes characteristics. *Russ J Electrochem* 52(7):613–621
 44. Somalu MR, Muchtar A, Brandon NP (2017) Properties of screen-printed nickel/scandia-stabilized-zirconia anodes fabricated using rheologically optimized inks during redox cycles. *J Mater Sci* 52(12):7175–7185
 45. Bebelis S, Neophytides S (2002) AC impedance study of Ni-YSZ cermet anodes in methane-fuelled internal reforming YSZ fuel cells. *Solid State Ionics* 152:447–453
 46. Mahata T, Nair S, Lenka R, Sinha P (2012) Fabrication of Ni-YSZ anode supported tubular SOFC through iso-pressing and co-firing route. *Int J Hydrog Energy* 37(4):3874–3882
 47. Mermelstein J, Millan M, Brandon N (2010) The impact of steam and current density on carbon formation from biomass gasification tar on Ni/YSZ, and Ni/CGO solid oxide fuel cell anodes. *J Power Sources* 195(6):1657–1666
 48. Seyednezhad M, Rajabi A, Muchtar A, Somalu MR (2015) Characterization of IT-SOFC non-symmetrical anode sintered through conventional furnace and microwave. *Ceram Int* 41(4): 5663–5669
 49. Ideris A, Croiset E, Pritzker M (2017) Ni-samarium-doped ceria (Ni-SDC) anode-supported solid oxide fuel cell (SOFC) operating with CO. *Int J Hydrog Energy* 42(14):9180–9187
 50. Buccheri MA, Singh A, Hill JM (2011) Anode-versus electrolyte-supported Ni-YSZ/YSZ/Pt SOFCs: effect of cell design on OCV, performance and carbon formation for the direct utilization of dry methane. *J Power Sources* 196(3):968–976
 51. Mahmud LS, Muchtar A, Somalu MR, Jais AA (2017) Processing of composites based on NiO, samarium-doped ceria and carbonates (NiO-SDCC) as anode support for solid oxide fuel cells. *Process Appl Ceramics* 11(3):206–212
 52. Kusnezoff M, Trofimenko N, Müller M, Michaelis A (2016) Influence of electrode design and contacting layers on performance of electrolyte supported SOFC/SOEC single cells. *Materials* 9(11): 906
 53. Uma K, Chu CH, Pan GT, Yang TC, Wang SF (2018) Hydrogen production of nickel-scandia-stabilized zirconia and copper/nickel-scandia-stabilized zirconia catalysts through steam methane reforming for solid oxide fuel cell operation. *Clean Techn Environ Policy* 20(9):2067–2074
 54. Awadallah AE, Mostafa MS, Aboul-Enein AA, Hanafi SA (2014) Hydrogen production via methane decomposition over Al_2O_3 - TiO_2 binary oxides supported Ni catalysts: effect of Ti content on the catalytic efficiency. *Fuel* 129:68–77
 55. Cho CK, Lee KT (2013) Characterization of $\text{Ni}_{1-x}\text{Cu}_x\text{Ce}_{0.8}\text{Gd}_{0.2}\text{O}_{1.9}$ composite anodes for methane-fueled solid oxide fuel cells. *J Ceram Process Res* 14(1):59–64
 56. Guo Y, Wan T, Zhu A, Shi T, Zhang G, Wang C, Yu H, Shao Z (2017) Performance and durability of a layered proton conducting solid oxide fuel cell fueled by the dry reforming of methane. *RSC Adv* 7(70):44319–44325